Available online at www.sciencedirect.com

ScienceDirect

Energy Procedia 45 (2014) 1136 – 1145

Energy Procedia

68th Conference of the Italian Thermal Machines Engineering Association, ATI2013

Evaluating the Performance of a Rotary Vane Expander for Small Scale Organic Rankine Cycles using CFD tools

Gianluca Montenegro[a,*], Augusto Della Torre[a], Marco Fiocco[a], Angelo Onorati[a], Christian Benatzky[b], Gerd Schlager[b]

[a]*Politecnico di Milano, Department of Energy , Via Lambruschini 4, Milano 20156, Italy*
[b]*Magna Powertain, Engineering Center Steyr, Steyrer Strasse 32; 4300 St. Valentin, Austria*

Abstract

This work proposes a focus on the simulation of a rotative volumetric expander via a CFD code. A customized application of OpenFOAM® has been developed to handle the particular motion of the calculation grid. In particular, a prescribed shape of the stator has been defined in order to adapt the motion of the vanes along the whole cycle. The model uses a mesh to mesh interpolation technique, switching from a calculation grid to the new one on the basis of dynamic mesh quality considerations.
This particular approach allows to account for the presence of leakages occurring between the stator and vane tips and also occurring at the top and bottom of the vanes. The fluid considered is the refrigerant R245fa, whose particular properties have been determined resorting to the NIST database. Experimental data, measured at different conditions of mass flow and fluid temperature, are compared to calculation results. Moreover, the CFD analysis has allowed the estimation of the influence of the leakage mass flow occurring at the tip of the vanes on the overall machine performances.

Keywords: CFD, rotary volumetric machine, ORC, real gas behavior

1. Introduction

The trends of rising fuel costs and the necessity of reducing CO_2 emissions is forcing governments and industries to focus on the development of low temperature heat energy recovery systems. One of the largest sources of waste energy is the internal combustion (IC) engine used in different vehicles (naval ship, railway, automotive, etc.).
The IC engine converts approximately one third of the combustion power into mechanical power [1]. The remaining power is distributed throughout multiple heat exchangers or is directly released to the ambient at the tail pipe. An ORC could be one measure to increase the overall efficiency of an ICE by using the waste heat from the exhaust or the coolant. The ORC consists of the classical steam generation in a Rankine cycle using an organic working fluid instead of water. The organic fluid is usually characterized by low saturation temperatures and by a saturated vapor line with positive slope in the T-s diagram. This positive slope prevents the formation of a two-phase mixture during

* Corresponding author. Tel.: +39 02 2399 8639 ; fax: +39 02-2399 8650.
E-mail address: gianluca.montenegro@polimi.it

doi:10.1016/j.egypro.2014.01.119

the expansion process through the expansion. The adoption of an ORC technology on an internal combustion engine may suffer the unsteadiness of the conditions at which the engine operates (low and high load). This difficulty can be overcome adopting a volumetric expander instead of a traditional thermal machine which may experience dramatic efficiency losses due both to the small size of the device and to the variable thermodynamic conditions of the working fluid. Examples of application of volumetric expanders involve Scroll machines or rotary vane machines. They are characterized by good efficiency, small vibration, low acoustic impact, simple and reliable structure and are well consolidated machines since they are used as compressors in refrigeration systems and heat pump systems from many years [2].
Theoretical studies showing the potentialities of the waste heat source recovery system in vehicles are present in the literature [3,4]. A comprehensive evaluation of all the heat sources at each operating points of an internal combustion engine and a selection of the waste heat sources is presented in [4]. Works focused on the experimental characterization of expanders have been published in the literature in the attempt to determine the thermodynamic and the volumetric efficiency under different operating conditions [5,6]. Theoretical works are also focused on the formulation of numerical models based on 1D considerations [7–10]. On the contrary, there are no examples of application of CFD models applied to the study of full scale fluid dynamics of vane expanders.
The present work focuses on the description of a strategy to perform a full cycle simulation of a rotary vane expander working with an organic fluid. Particular attention has been paid to the mesh generation and mesh motion strategy, since the small gaps characterizing this type of machines are difficult to be captured and handled when the vane motion is modeled. The leakage is considered to be present all around the vanes (radial and axial direction) and its impact on the power production has been evaluated.
The CFD code adopted is a customized version of the open source code OpenFOAM [11]. The developed code has been applied to the full scale simulation of multiple cycles of a dual chamber rotary vane expander and the result compared to experimental measurements.

2. CFD approach

The purpose of this work is to present a CFD procedure for the prediction and optimization of fluid dynamic performances of volumetric machines dedicated to the power production inside ORC cycles. The CFD modeling of rotary vane machines is a quite challenging task to perform. In particular, there are issues related to the handling of the mesh motion, to the mesh generation and to the treatment of the gas behavior.
The mesh handling and generation must be carefully performed in order to preserve the mesh quality at each crank angle of the thermodynamic cycle. Additionally, this type of machine relies on the interaction between the vanes and the stator to mimic the sealing effect that in alternative volumetric machines is realized by means of specific sealing rings. This means that tiny gaps between static components and rotating ones must be taken into account to evaluate the effects of intra chamber leakages.

2.1. Governing equations

In order to describe the fluid-dynamics problem, the system of conservation equations for the generic continuum needs to be combined to the constitutive relations describing the properties of the specific medium. This allows to close the mathematical system of governing equations. The governing equations for the generic continuum are the conservation of mass, momentum and energy applied to a compressible single phase fluid also known as the Navier-Stokes equations:

- Continuity equations, which states the conservation of mass:

$$\frac{\partial \rho}{\partial t} + \nabla \cdot (\rho \mathbf{U}) = 0 \tag{1}$$

- Navier-Stokes equations, derived from the conservation of momentum (linear and angular):

$$\frac{\partial \rho \mathbf{U}}{\partial t} + \nabla \cdot (\rho \mathbf{U}\mathbf{U}) = \rho \mathbf{g} - \nabla \left(p + \frac{2}{3}\mu \nabla \cdot \mathbf{U} \right) + \nabla \cdot \left[\mu \left(\nabla \mathbf{U} + \nabla \mathbf{U}^T \right) \right] \tag{2}$$

- Energy equation:

$$\frac{\partial \rho e}{\partial t} + \nabla \cdot (\rho e \mathbf{U}) = \rho \mathbf{g}\mathbf{U} - \nabla \cdot (p\mathbf{U}) - \nabla \cdot \left[\frac{2}{3}\mu (\nabla \cdot \mathbf{U})\mathbf{U} \right] + \nabla \cdot \left[\mu \left(\nabla \mathbf{U} + \nabla \mathbf{U}^T \right) \mathbf{U} \right] + \nabla \cdot (\lambda \nabla T) + \rho Q \tag{3}$$

2.2. Real gas effect

Working fluids of Rankine cycles can be well represented resorting to the simplest equation of state, namely the ideal gas equation. An ideal gas is defined as one in which all collisions between molecules are perfectly elastic and in which there are no intermolecular attractive forces. Typically, in ORC systems the beginning of the expansion occurs at conditions close to the critical pressure, where the intermolecular effects are increased. Because of these deviations, the study of the expansion of an organic fluid must not be studied with the ideal gas law. On the other hand, when pressures and temperatures decrease below the critical zone, the intermolecular effects are becoming increasingly negligible, thus reducing the deviation from the ideal gas behavior.

The working fluid considered in this work is the hexafluoropropane refrigerant (R245fa), derived from the propane molecule by partially substituting hydrogen with atoms of Fluor (F). This particular type of fluid offers a saturated vapor curve which is particularly favorable for expansion at low temperature.

There are several ways of modeling real gas effects for refrigerants of varying complexity [12,13]. They can be used to model the thermophysical properties in conditions where the ideal assumptions can not be considered. The Redlich-Kwong-Soave and the Peng-Robinson equation of state have shown to provide a good approximation of the real gas effect when evaluating thermo-physical state of organic fluids [3,12]. The same equations can be used in the CFD to determine the density from the pressure and temperature field at every fluid cell. The adoption of these equations requires the inclusion of extra terms when integrating the thermodynamic variables to get the values of enthalpy and internal energy [3].

In this work an alternative approach, based on the adoption of lookup tables, has been adopted in order to determine the thermo dynamic state. The procedure is based on a script capable of generating discrete tables of properties from the NIST database. The tabulated data are then accessed during the simulation, resorting to linear interpolation when the required value falls within two tabulated data. This procedure allows also to highlight a possible risk of liquid formation when the thermodynamic state falls below the saturation curve. Examples of interpolated 2D tables for two different fluid properties, namely density and enthalpy, are shown in Figure 1.a and Figure 1.b.

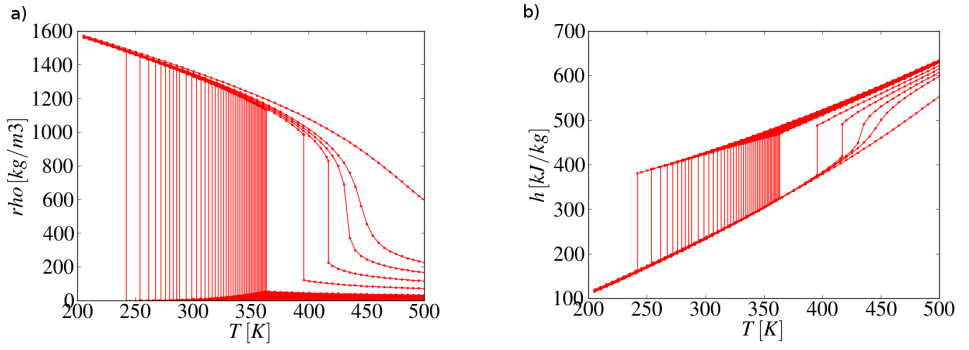

Fig. 1. (a) Tabulated density at a fixed pressure level; (b) Tabulated enthalpy at a fixed pressure level.

2.3. Mesh generation and handling

The mesh handling adopted in this work is based onto a mesh to mesh interpolation combined with boundary motion and deformation. The basic concept is that mesh can be generated for one specific crank angle. The mesh motion is then imposed to the boundaries (all the patches composing the rotor boundary) as a composition of a rigid rotation plus a radial translation (radial motion of the vanes). The inner points of the mesh are therefore moved in order to adapt to the boundary motion (mesh deformation). Usually, when the mesh is deformed, its quality decreases: skewness, non orthogonality and mesh cell geometry validity are checked. As a consequence, when the deformation becomes excessive a new mesh must be created and the solution mapped from the old mesh onto the new one thorough field interpolation techniques. Due to the small entity of the tiny gaps, the angular step that can be covered with a single mesh is usually very small, few tenths of a grade.
A possible strategy could be the generation of the entire set of meshes a priori, keeping constant the angular validity of every mesh during the whole cycle. In this case, the safest solution would be to set the angular step to small values, in order to guarantee the quality of every mesh for every vane position. The result can be a large number of meshes to deal with and a consequent huge demand of memory usage. Another drawback is that the field remapping operation must be performed several times, resulting in a overhead comparable to the computational one. Moreover, the generation of a large set o meshes can be severely limiting if every single mesh must be generated manually, unless an automatic mesh generator is adopted. For this reason in this work it has been implemented a mesh generation strategy in which the angular validity of every mesh is determined on the basis of mesh quality indexes.
The mesh is created automatically resorting to a built-in cartesian mesh generator. It is then moved to reach the maximum revolution angle compatible with mesh quality requirements. The angular position relative to the last valid mesh is then set as the angle at which the mesh switch must be performed.
At this point a new mesh is generated for the new angle and the procedure is repeated until the whole cycle is swept. To reduce the time required for the generation of every single mesh, it has been developed a parametric ”base mesh” that is exploited every time a new mesh must be created.

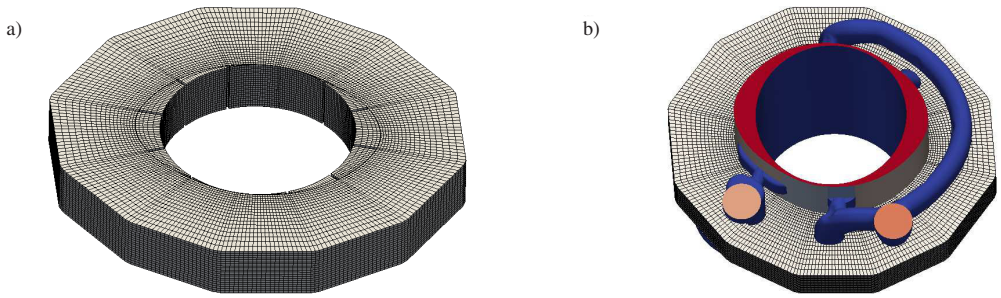

Fig. 2. (a) Initial parameterized base mesh; (b) Inclusion of the real machine surface for mesh creation.

2.4. Base mesh generation

The base mesh is generated on the basis of the revolution angle by means of a parametric script which, given the number of vanes, the mesh size and the entity of the gaps, creates a structured mesh oriented in the radial direction (Figure 2.a). In order to preserve a high mesh quality as much as possibile, the base mesh is generated for every angle at which the mesh is switched, following the rotation of the shaft. In Figure 2 it is shown how a slice of rotor mesh is created for a fixed angle and how it overlaps with the surface representation of the whole machine. Once the base mesh has been created, the next step of the automatic meshing procedure is the selection of the cells needed to reproduce the fluid region and the adaption of the cell vertexes to the surface of the geometry. To do this a surface file describing the machine geometry is superimposed to the base mesh, as shown in Figure 2.b, and all the cells of the base mesh falling outside of the surface are removed. A refinement step is then added to increase the mesh resolution around the featuring edges of the geometry and around the vane tips. The final step is the adaption of the mesh points to the real surface. This step produces a deformation, and consequently a decrease of quality, of the mesh in order to resolve the

edges of the machine. An example of the final result of the meshing process is illustrated in Figure 3.a, where it is possible to see that both the vane tip/stator and top/bottom leakages are considered. The main assumption in this case is that the leakage is assumed to be constant at a fixed operating condition. This assumption is realistic for the leakage between the top/bottom of the vanes and the top/bottom walls of the machine, but not for the vane tip/stator leakage. As a matter of fact, the latter is a resultant of the balances of the forces acting on the vane in the radial direction and is a function of the revolution speed as well as of the vane angular position and inertia [14]. The present work assigns a constant value, the order of magnitude of tens of microns, to the tip vane leakage, according to values suggested by the manufacturer, and relies on the adoption of porous media approaches to calibrate the leakage for specific revolution speed. Because of this simplification, the usage of fluid-structure interaction to determine the leakage can be avoided during the calculations. The rotation of the base mesh for the generation of the new mesh becomes very useful also to facilitate the remapping of the solution. This operation can be performed without introducing errors only if the target and the source meshes are perfectly matching in terms of boundary position. The rotation of the base mesh allows to have the vane edges of the source mesh and of the target meshes positioned exactly at the same location. Conversely, an automatic mesh generation performed with a fixed base mesh, regardless of the crank angle, would have produced an edge resolution dependent from the vane angular position (different way of cutting the base mesh) leading to mismatching positions of the boundary points between the target and the source meshes.

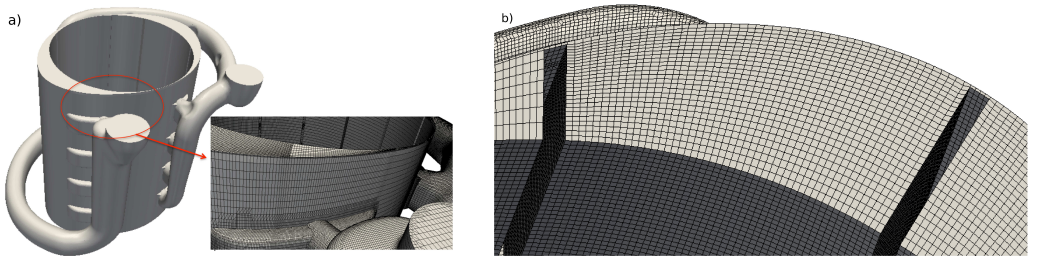

Fig. 3. (a) Final mesh of the whole machine ; (b) Detail of the vane stator gap.

2.5. Motion algorithm

Since the leakages need to be modeled, the mesh resolution must adapt to the smallest gap of the geometry. The resulting calculation grid will be very refined around the machine vanes and progressively coarsened towards the bulk of the chamber, in order not to increase excessively the cell number. The point motion is imposed at the boundaries of the system, namely the vanes and the shaft. In particular, the imposition of the shaft motion is trivial and consist in assigning a new position to the boundary points according to a rigid rotation by an angle resulting from the revolution speed and the selected time step. For what concerns the points belonging to the vanes, their motion needs to be determined not only as a function of the rotation speed but also as function of their angular position. The possibility of customizing the stator profile to realize the desired variation of volume, imposes to add a rigid radial translation of the vanes in addition to the rigid rotation around the rotor axis. The stator profile law is input as a polar coordinate diagram in which the radial distance of the points is function of the angle. A profile law defined with a resolution of 1.0 degree may be sufficient to describe the stator profile for small sized machines. The positioning of mesh points between two near angular positions is determined via linear interpolation.
As shown in Figure 3.b the vane tip is not rotated and displaced rigidly but is is also deformed in order to keep the gap constant during a complete rotation. The point belonging to the vane side are therefore translated proportionally to their distance from the tip.
The remaining vertexes, those not falling on moving boundaries, must adapt their position in order to follow the boundary motion and to preserve the mesh validity. A typical algorithm for the internal point motion is based on the solution of the point diffusivity equation. Points are therefore moved solving a diffusion point motion equation as follows:

$$\gamma \nabla^2 \mathbf{x} = 0, \tag{4}$$

where the coefficient γ is the diffusion coefficient that is evaluated according to the inverse of the distance from the points to specified boundary patches. This means that points close to specific patches are moved similarly to boundary nodes, points far from the boundary patches are moved with a small displacement. The position of the points at the new time step is then determined in the following way:

$$\mathbf{x}_{new} = \mathbf{x}_{old} + \Delta\mathbf{x}. \tag{5}$$

After the mesh motion, the mesh flux determined by the face swept volume is included in the governing equations 1-3 and the solution fields are calculated at the new time step [15,16]. This procedure is repeated referring to a single mesh until mesh quality criteria are satisfied. When the mesh switch must be operated, all the fields are remapped on the new mesh resorting to second order interpolation techniques.

2.6. Flow resistance model

The solution of the flow through the leakage at the vane tip requires the adoption of a very refined mesh, in order to correctly capture the velocity profile in the tiny gap between the vane and the housing. However, this approach would lead to a significant increase of the computational burden of the simulation. Therefore other approaches need to be followed, especially when the CFD is applied in the context of an industrial framework. For that reason, in this work a flow resistance model has been adopted for the description of the leakage at the vane tip. The momentum equation 2 has been modified by the introduction of a Darcy-Forchheimer type source term, which takes into account both the viscous and inertial effects occurring in the tiny gap:

$$\mathbf{S} = -\left(\mu d + \frac{\rho|\mathbf{U}|}{2} f\right)\mathbf{U} \tag{6}$$

This resistance source term is applied locally only on the cells located at the tip of the vane and included in the momentum equation (Equation 2).

3. Expander type and test rig

In this paper a dual chamber rotary vane machine has been considered to convert the thermal power to mechanical power. Such a machine is generally consisting of a stator, a rotor and a certain number of vanes which are moveable in radial direction. A simple sketch of the expander is shown in Figure 4.a.

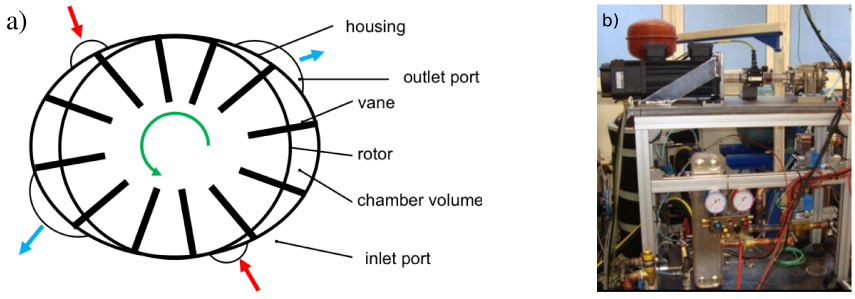

Fig. 4. (a) Schematic of the dual chamber radial expander; (b) Picture of the test rig used for the measurement campaign.

An expander chamber is formed by two adjacent vanes, the rotor and the housing. In the axial direction the chamber is sealed by cover plates. The vane expander considered in this study is a dual chamber machine and therefore the cycle frequency is two times the revolution frequency. The complete cycle (inlet, expansion, outlet) is realized in 180° of the circumference and then the cycle is repeated during the second 180°, resulting in a double specific power output with respect to a single inlet-outlet machine. Moreover, this symmetry causes the resultant of the radial forces acting on the shaft to cancel out.

The stator has been designed following a specific profile capable of realizing the desired expansion. The position of the inlet and outlet ports has been determined in order not to over-expand the vapor, avoiding in this way pumping losses. Figure 4.b shows the test bench setup used to perform the experimental measurements. At the top the expander is connected, via a torque measurement flange, to an electric motor/brake. For basic investigations the refrigerant R245fa has been used as a working fluid. The facility has been set up to perform different efficiency maps (isentropic, volumetric, system efficiency) and also dynamic experiments like NEDC, WLTP cycles can be performed.

4. CFD Simulations

The volumetric expander has a radial layout, with the inlet and outlet ports located on the external stator profile. In particular, the ports are positioned in four locations in the axial direction, as shown in Figure 5.a. This layout made possible a reduction of the size of the computational domain, where only the portion of the machine competing to a single group of inlet/outlet ports has been considered. The resulting computational mesh, highlighted in blue in Figure 5.a, consists of $5 \cdot 10^5$ cells.

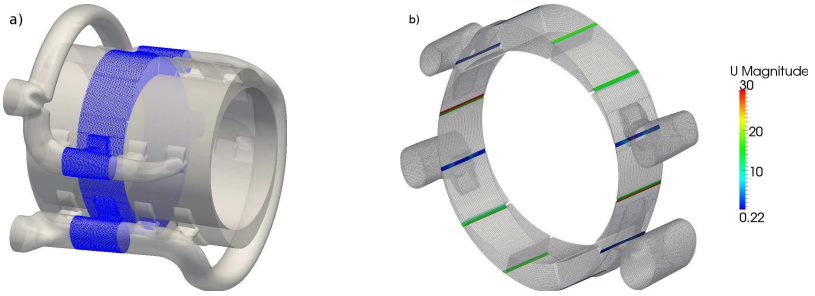

Fig. 5. (a) Computational domain used for the simulations; (b) Definition of the cell regions for the modeling of the vane tip leakage.

Simulations were run considering different operating conditions at variable rotational speed, mass flow and temperature of the fluid at the inlet. The parameters adopted in the simulation campaign are listed in Table 4. For confidentiality reasons, the values of the parameters presented in the following sections are non-dimensionalized with respect to a reference condition.

Table 1. Operating conditions considered in the simulations.

	Rotational speed $\left[min^{-1}\right]$	Mass flow [−]	Inlet temperature [−]
OC0	1250	1.000	1.000
OC1	1000	1.060	0.995
OC2	750	0.810	1.002

As previously stated, in order to correctly describe the leakage flow occurring at the tip of the vanes, a flow resistivity source term has been introduced. The set of cells where the resistivity model is applied is highlighted in Figure 5.b, where cells are colored according to the magnitude of the velocity field. Simulations were run considering different values for the parameters of the flow resistance model, in order to investigate the influence of the leakage on the machine performances. For clarity sake, the parameters adopted in the simulations are listed in Table 4.

4.1. Results

In Figures 6 and 7 the computed thermo-dynamic fields, sampled on a slice located in the middle of the domain, are reported for the case OC0 - RM0. Considering the pressure field (Figure 6.a), it can be noticed that the fluid is expanded by the rotation of the machine vanes in counter-clockwise direction, from the inlet ports to the outlet ones. The velocity field in Figure 6.b shows the leakage between adjacent vanes, which is particularly strong for

Table 2. Parameters of the leakage flow resistance model adopted in the simulations.

	d $\left[m^{-2}\right]$	f $\left[m^{-1}\right]$
RM0	$1 \cdot 10^{10}$	$1 \cdot 10^{5}$
RM1	$2 \cdot 10^{9}$	$2 \cdot 10^{4}$
RM2	$1 \cdot 10^{9}$	$1 \cdot 10^{4}$

high pressure difference. Moreover, a flow directed from the inlet to the outlet ports, passing in clockwise direction through the tiny gap between rotor and stator, can be seen. This leakage flow can be noticed also by examining the temperature field (Figure 7.a), which shows a high temperature stream flowing from the inlet to the outlet zone. In these simulations a thermophysical model based on a database of tabulated properties was adopted for describing the real gas behavior of the organic fluid. Figure 7.b shows the compressibility factor field, highlighting non-negligible deviations from the perfect gas model behavior in regions characterized by high pressures and densities.

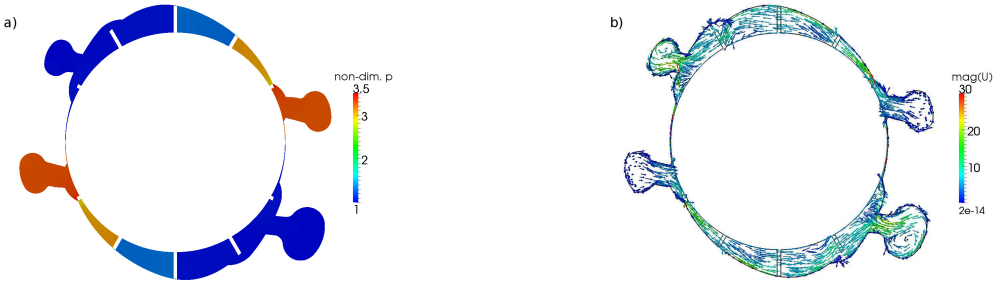

Fig. 6. (a) Cut plane of the computed pressure field; (b) Cut plane of the computed velocity field.

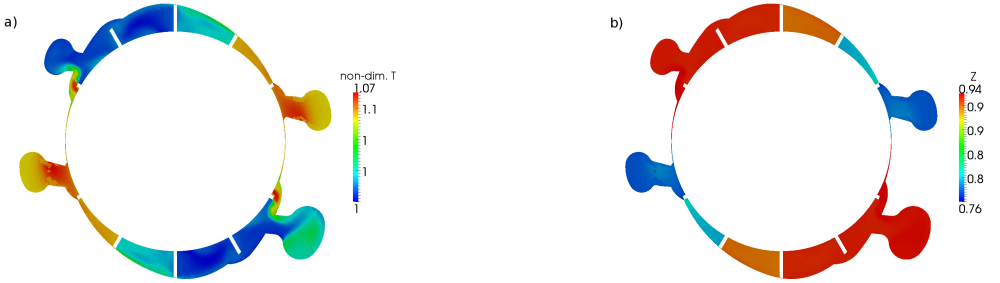

Fig. 7. (a) Cut plane of the computed temperature field; (b) Cut plane of the computed compressibility factor.

The power output of this machine is plotted in Figure 8.a as function of the crank angle, for three different operating conditions: OC0, OC1, OC2. For all this cases the RM0 parameters are used in the leakage flow resistance model. It can be seen that, after a complete revolution (360°), the calculated power has reached a regime condition. The regime power output has a linear dependence on the mass flow, exhibiting higher values for case OC1 and lower for case 0C2. Figure 8.b reports the pressure traces probed at the inlet section of the machine: also this quantity seems to reach the regime value after one cycle revolution.

In Figure 9.a the temperature at the outlet sections is plotted. It can be seen that after 180° the temperature begins to decrease, since the fluid, entering in the machine at high temperature, is expanded in the rotating vanes and then is discharged at a lower temperature. Figure 9.b shows the variation of the mass flow through the leakage at the vane tip during a rotation of 30°.

The leakage occurring at the tip of the vane has a direct influence on both the machine power output and the back-

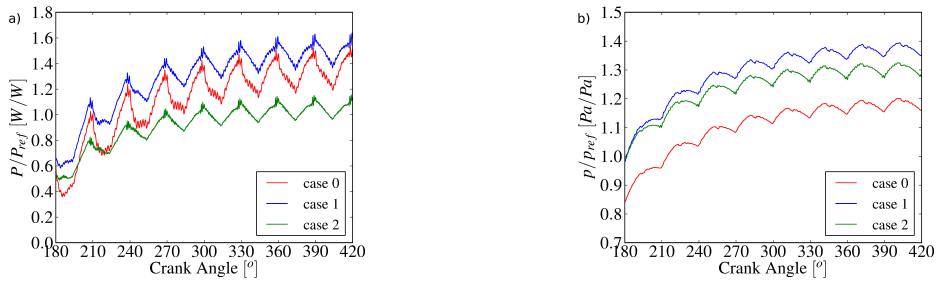

Fig. 8. (a) Non dimensional computed power output; (b) Non dimensional computed inlet pressure.

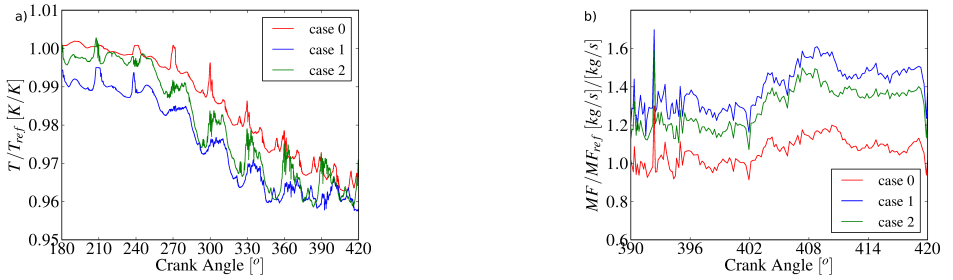

Fig. 9. (a) Calculated non dimensional temperature trace at the outlet of the expander; (b) Calculated non dimensional average leakage mass flow per vane.

pressure at the inlet. In Figure 10.a the power output, calculated using different values of the parameters for the resistance model, is plotted as function of the inlet pressure. Each curve is related to an operating condition where the flow resistance (applied in the leakage zone) increases moving from the left to the right. Moving towards higher values of flow resistance a better volumetric efficiency of the machine is obtained. Measured data are reported for the three different operating condition considered: it can be seen that simulations approach the experimental data for certain values of the flow resistance parameters. At this stage the CFD model can not be considered predictive, since calibration of the model is needed; however the simulations can provide information about the influence of the volumetric efficiency on the machine performances. For example, Figure 10.b illustrates the dependency of the machine power output on the mass flow through the vane tip leakage.

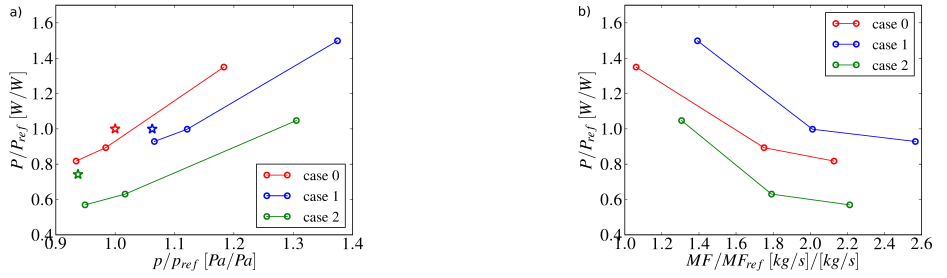

Fig. 10. (a) Machine power output as function of the inlet. On each curve, RM2, RM1, RM0 parameters are applied moving from the left to right. Stars indicate measured values ; (b) Machine power output as function of the leakage mass flow on the vane tip.

5. Conclusions

This work describes a CFD simulation of a vane expander machine adopted as power source inside an organic Rankine cycle. The particular mesh handling and mesh generation strategies have allowed the prediction of the indicated power output of a dual chamber vane expander. Simulations have been carried out considering three different operating conditions, and results have been compared to measured data, showing an encouraging agreement. All the simulations were carried out modeling the effect or real gas, which, in particular at the intake side, shows a variation from the perfect gas law of 30% for the conditions studied in this work. Moreover, the presence of leakages between the vane tip and the stator has allowed an estimation of the influence of the volumetric efficiency on the machine performances. The resistance coefficient used for the modeling of the leakage flow is a parameter that needs to be calibrated. A fully predictive model would require the calculation of the force balance of each vane. This means a mesh resolution at least one order of magnitude finer than the one used in the present approach, leading to a computation runtime that can be coped with only by resorting to massive parallelization.

References

[1] Heywood, J.B.. Internal Combustion Engine Fundamentals. McGraw-Hill; 1988.
[2] Guangbin, L., Yuanyang, Z., Liansheng, L., Pengcheng, S.. Simulation and experiment research on wide ranging working process of scroll expander driven by compressed air. Applied Thermal Engineering 2010;30(1415):2073 – 2079. doi:http://dx.doi.org/10.1016/j.applthermaleng.2010.05.015.
[3] Lujn, J., Serrano, J., Dolz, V., Snchez, J.. Model of the expansion process for {R245fa} in an organic rankine cycle (orc). Applied Thermal Engineering 2012;40(0):248 – 257. doi:10.1016/j.applthermaleng.2012.02.020.
[4] Macin, V., Serrano, J., Dolz, V., Snchez, J.. Methodology to design a bottoming rankine cycle, as a waste energy recovering system in vehicles. study in a {HDD} engine. Applied Energy 2013;104(0):758 – 771. doi:http://dx.doi.org/10.1016/j.apenergy.2012.11.075.
[5] Xia, C., Zhang, W., Bu, G., Wang, Z., Shu, P.. Experimental study on a sliding vane expander in the {HFC410A} refrigeration system for energy recovery. Applied Thermal Engineering 2013;59(12):559 – 567. doi:10.1016/j.applthermaleng.2013.05.050.
[6] Gnutek, Z., Kolasinski, P.. The application of rotary vane expanders in organic rankine cycle systems - thermodynamic description and experimental results. Journal of Engineering for Gas Turbines and Power 2013;135(6).
[7] Wang, M., Cao, F., Zhao, Y., Wang, Z., Bu, G.. Comparison between modeling and experiments on a two-stage rotary vane expander for an hfc-410a air conditioning system. Proceedings of the Institution of Mechanical Engineers, Part A: Journal of Power and Energy 2013;227(2):193–205. doi:10.1177/0957650912470913.
[8] Mahmoud, A.M., Sherif, S.A., Lear, W.E.. Frictional and internal leakage losses in rotary-vane two-phase refrigerating expanders. Journal of Energy Resources Technology, Transactions of the ASME 2010;132(2):0210071–02100710.
[9] Subiantoro, A., Ooi, K.. Analysis of the revolving vane (rv-0) expander, part 2: Verifications of theoretical models. International Journal of Refrigeration 2012;35(6):1744–1756.
[10] Wang, M., Zhao, Y., Cao, F., Bu, G., Wang, Z.. Simulation study on a novel vane-type expander with internal two-stage expansion process for r-410a refrigeration system. International Journal of Refrigeration 2012;35(4):757 – 771. doi:10.1016/j.ijrefrig.2011.11.014.
[11] Weller, H.G., Tabor, G., Jasak, H., Fureby, C.. A Tensorial Approach to CFD using Object Orientated Techniques. Computers in Physics 1998;Vol. 12(No. 6):620.
[12] Brown, J.S.. Predicting performance of refrigerants using the pengrobinson equation of state. International Journal of Refrigeration 2007;30(8):1319 – 1328. doi:10.1016/j.ijrefrig.2007.04.006.
[13] Colonna, P., Rebay, S., Harinck, J., Guardone, A.. Real gas effects in orc turbine flow simulations: influence of thermodynamic models on flow fields and performance parameters. Proceedings of the ECCOMAS CFD 2006 Conference 2006;.
[14] KIM, H.J., KIM, W.Y., AHN, J.M., CHO, S.O.. Numerical study on the performance improvement of a rotary vane expander for a co2 heat pump cycle. International Journal of Air-Conditioning and Refrigeration 2011;19(04):311–319. doi:10.1142/S2010132511000648.
[15] Ferziger, J.H., Perić, M.. Computational methods for fluid dynamics. Springer; 1997.
[16] Versteeg, H.K., Malalasekera, W.. An Introduction to Computational Fluid Dynamics: the Finite Volume Method. Addison-Wesley, Longman; 1995.